SUPPORTING INFORMATION

Insights into Cr/SiO$_2$ catalysts during dehydrogenation of propane: an *operando* XAS investigation

M. Botavina,[a] C. Barzan,[a] A. Piovano,[a] L. Braglia,[a] G. Agostini,[b] G. Martra,[a] and E. Groppo[a*]

Additional details on the EXAFS data analysis for 1-ox and 1-red samples

The EXAFS spectrum of **1-ox** was analysed using as input structure the model shown in Figure S1a, where the absorbing chromium site is in the form of a monochromate, characterized by two double-bonded oxygen ligands and grafted to the silica surface through two single-bonded Cr-O ligands.
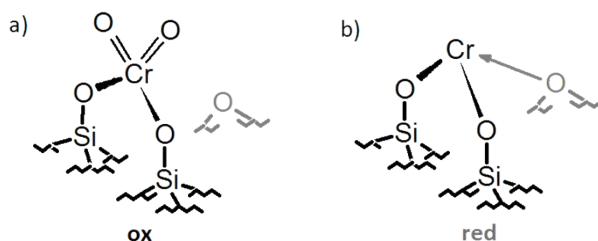

Figure S1 – Schematic representation of surface chromates (part a) and Cr^{II} sites (part b) anchored at the silica surface.

A first shell analysis was performed by optimizing the following parameters:

i)   a single ΔE_0 common to all the paths;

ii) a single S_0^2 value; the coordination numbers for both ligands ($N_{Cr=O}$ and N_{Cr-O}) were both fixed to 2;

iii) the two Cr-O distances ($R_{Cr=O}$ and R_{Cr-O}, respectively).

iv) two Debye-Waller factors for the two ligands ($\sigma^2_{Cr=O}$ and σ^2_{Cr-O}, respectively).

The quality of the fit can be appreciated in Figure S2, where the contributions of the two oxygen ligands is also shown; a summary of the fit results is given in Table 3 of the main text.
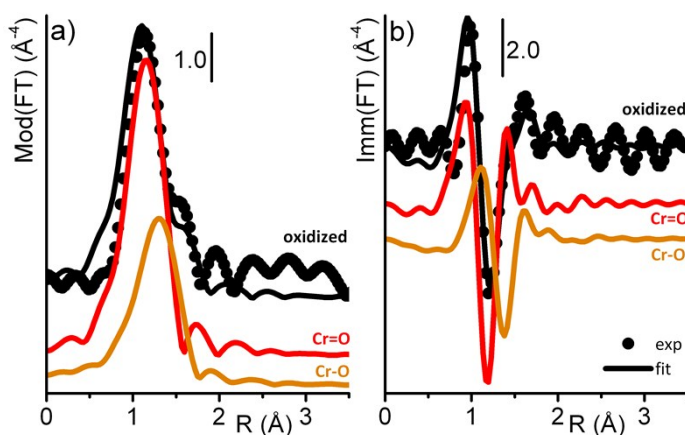

Figure S2 – Phase-uncorrected Fourier Transform (FT) of the $k^3\chi(k)$ EXAFS function for **1-ox**, in both modulus and imaginary parts (parts a and b, respectively); the experimental datum (circles) is overlapped to the best fit (full line). Also the two scattering paths that contribute to the first-shell experimental signal are reported (vertically translated for clarity).

The analysis of the spectrum for **1-red** was less straightforward. As a matter of fact, the very small amplitude of the EXAFS oscillations in the k^3-weighted $\chi(k)$ functions implies a low accuracy in the determination of the coordination numbers. It was not possible to fit the datum by leaving free all the fitting variables. Therefore, the fit was performed by fixing S_0^2 to the value found for the oxidized sample. The best fit was obtained by considering, in addition to the ligands shown in

Figure S1b, also one oxygen ligand at a slightly longer distance. The quality of the fit can be appreciated in Figure S3, where the contributions of the relevant paths is also shown. A summary of the fit results is given in Table 3 in the main text.
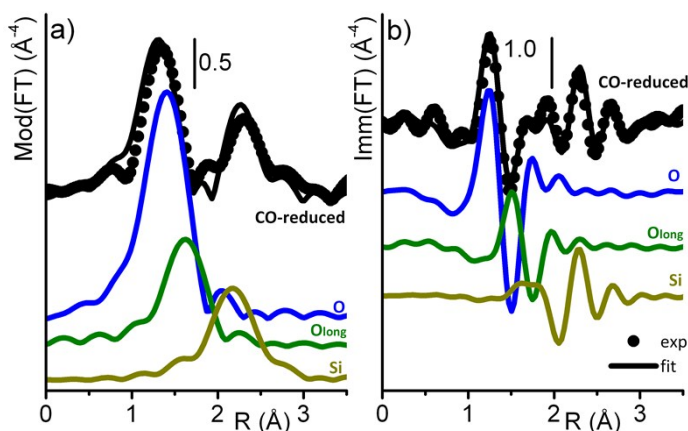

Figure S3 – Phase-uncorrected Fourier Transform (FT) of the $k^3\chi(k)$ EXAFS function for **1-red**, in both modulus and imaginary parts (parts a and b, respectively); the experimental datum (circles) is overlapped to the best fit (full line). Also the three scattering paths that mainly contribute to the experimental signal are reported (vertically translated for clarity).

Additional details on the EXAFS data analysis for the catalysts recovered after propane dehydrogenation in different conditions

In the analysis of the EXAFS data it we took into account the fact that the XANES data demonstrate the presence of two different phases in all the samples, differing in both the oxidation state and coordination geometry. Therefore, a correct approach should imply a two-phases analysis. Nevertheless, we have also demonstrated that the EXAFS signal characteristic of the Cr^{II}-phase is much less intense than the oscillations of Cr^{III}-phase. Hence, we expect that the experimental signal of a mixture of Cr^{III} and Cr^{II}-phases should be dominated by the Cr^{III}-phase. For this reason, we performed a preliminary data analysis by considering only the Cr^{III}-phase contribution. In a second moment, we improved the level of calculation by performing a two phase analysis. The two approaches will be discussed separately.

Single phase analysis
In a preliminary attempt, we performed an analysis by considering the presence of a Cr^{III}-phase only. For the first three catalysts (i.e. treated in the presence of propane only, propane +CO_2, and propane + O_2), the analysis was performed by using Cr_2O_3 as input structure and by considering two scattering paths only: a) a Cr-O for the first shell signal and b) a Cr-Cr path for the second shell signal. As a matter of fact, the absence in the Imm(FT) of the beats characteristic of Cr_2O_3 suggests that only one type of chromium ligand contributes to the second shell signal. In all the three cases, the fit was performed by optimizing the following parameters:
i)   a single ΔE_0 common to all the paths;

ii) the coordination numbers for both ligands (N_O and N_{Cr}, respectively); the resulting N values were re-normalized to the S_0^2 value obtained by fitting the signal of the Cr_2O_3 reference compound (0.7);

iii) the two Cr-L distance;

iv) two Debye-Waller factors for the two ligands (σ^2_O and σ^2_{Cr}, respectively).

The quality of the fits can be appreciated in Figure S4, Figure S5, and Figure S6, where the two scattering paths that contribute to the experimental signal are also reported. A summary of the fit results are given in Table S1, Table S2, and Table S3.
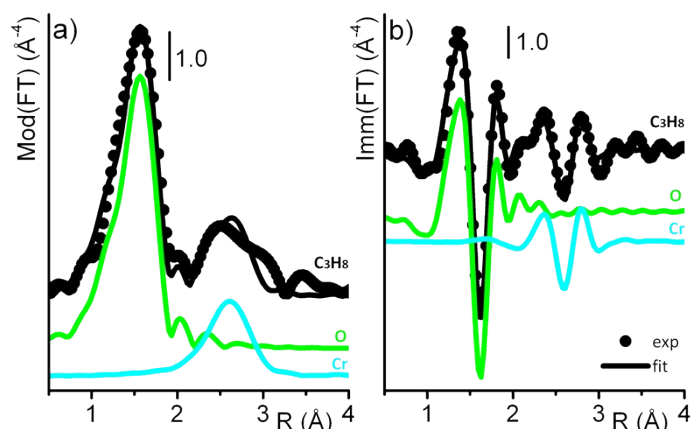

Figure S4 – Phase-uncorrected Fourier Transform (FT) of the $k^3\chi(k)$ EXAFS function for the catalyst **1-a**, in both modulus and imaginary parts (parts a and b, respectively); the experimental datum (circles) is overlapped to the best fit (full line). Also the two scattering paths that contribute to the experimental signal are reported (vertically translated for clarity).

Table S1 – Optimized parameters in EXAFS analysis (performed in the ΔR = 0.0 – 4.0 Å range, FT in 1.0–13.0 A^{-1} k-range) for catalyst **1-a**. The coordination numbers have been re-normalized to the S_0^2 value obtained by fitting the signal of the Cr_2O_3 reference compound (S_0^2 = 0.7). The fit resulted in R_{factor}= 0.035.

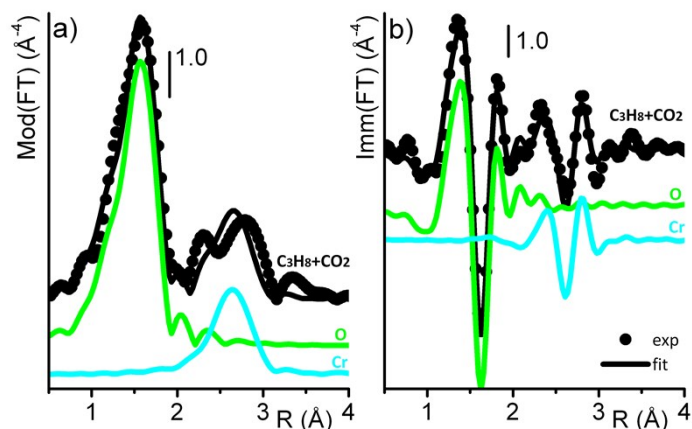|	ΔE (eV)	N	R (Å)	σ^2 (Å²)
O	0 ± 1	3.3 ± 0.3	2.009 ± 0.007	0.0057 ± 0.0009
Cr		1.9 ± 0.9	3.04 ± 0.02	0.012 ± 0.004

Figure S5 –As for Figure S4, for catalyst **1-b**.

Table S2 – As for Table S1 for catalyst **1-b**. The fit resulted in R_{factor}= 0.039.

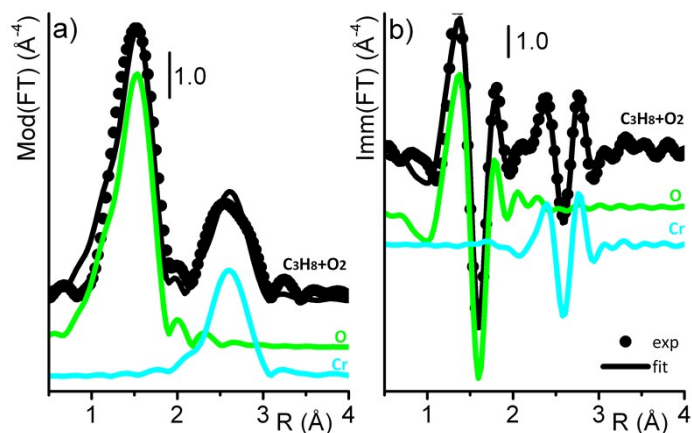|	ΔE (eV)	N	R (Å)	σ^2 (Å²)
O	0 ± 1	3.7 ± 0.3	2.017 ± 0.008	0.0058 ± 0.0009
Cr		1.6 ± 0.6	3.05 ± 0.02	0.009 ± 0.003

Figure S6 – As for Figure S4, for catalyst **1-c**.

Table S3 – As for Table S1 for catalyst **1-c**. The fit resulted in R_{factor}= 0.055.

	ΔE (eV)	N	R (Å)	σ^2 (Å²)
O	-2 ± 1	3.7 ± 0.4	1.985 ± 0.009	0.006 ± 0.009
Cr		1.5 ± 0.9	3.01 ± 0.02	0.006 ± 0.004

The spectrum of catalyst **1-d** was analysed by considering five scattering paths: a) a Cr-O path for the first shell; b) two Cr-Cr paths for the second shell; c) two Cr-Cr paths for the third shell. Indeed, the presence of the beats at about 2.1 Å and 2.9 Å suggests that two Cr-Cr paths contribute in the same ΔR region. The results of the fit are summarized in Table S4, and the quality of the fit can be appreciated by looking at Figure S7.
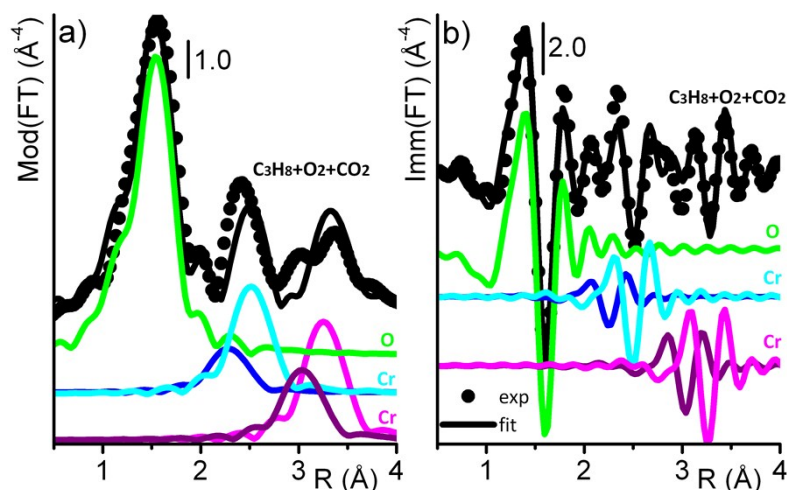

Figure S7 – As for Figure S4, for catalyst **1-d**.

Table S4 – As for Table S1, for catalyst **1-d**. The fit resulted in R_{factor}= 0.080.

	ΔE (eV)	N	R (Å)	σ^2 (Å²)
O		4.0 ± 0.7	1.98 ± 0.01	0.004 ± 0.001
Cr1	-3 ± 1	0.4 ± 0.2	2.68 ± 0.01	0.004 ± 0.002
Cr2		1.2 ± 0.2	2.91 ± 0.01	0.004 ± 0.002

In all the cases, although a single chromium phase was used to fit the experimental data instead of the two expected, the quality of the fits is good. In average: i) the first shell is composed of less than four oxygen ligands at an average distance of about 2.0 Å, to be compared with the six ligands at 1.995 Å in Cr_2O_3; ii) the second shell is constituted by less than two chromium ligands at an average distance of 3.0 Å, to be compared with three chromium at 2.90 Å + 1 Cr at 2.66 Å in Cr_2O_3. The Cr-Cr distances are close to those characteristic of Cr_2O_3 for the catalyst treated in the presence of all the reagents.

Although the first shell Cr-O distance is very close to that characteristic of Cr_2O_3, the average coordination number is smaller than that expected for O-terminated CrO_6 octahedra. This result is in agreement with the co-presence of a second phase (Cr(II)-like), where chromium sites are less coordinated than in Cr_2O_3, and at a slightly different distance.

Two phases analysis

In a second moment, we performed a two-phases analysis, considering the co-presence of a Cr^{II}-phase and a Cr^{III}-phase, having the following properties: i) the Cr^{II}-phase phase contributes only in the first shell signal with two oxygen ligands, being the corresponding signal quite weak; ii) the Cr^{III}-phase contributes to the first shell signal with six oxygen ligands, and also to the second shell one, with a number of chromium ligands that depends on the dimension of the Cr_2O_3-like particles. The fits were performed by considering 3 scattering paths: a) a Cr-O path for the Cr^{II}-phase, Cr-O_{II}; b) a Cr-O path for the Cr^{III}-phase, Cr-O_{III}; c) a Cr-Cr path for the Cr^{III}-phase contributing to the second shell signal. In all the cases, the fit was performed by fitting the following variables:

i)   a single ΔE_0 common to all the paths;

ii)   the fraction x of the Cr_2O_3-like phase, being defined as (1-x) the fraction of $Cr(II)/SiO_2$-like phase;

iii)   the amplitude of the Cr-Cr contribution, amp_Cr; from amp_Cr the N_{Cr} coordination number characteristic of the second shell around the absorbing sites can be obtained:

iv)   the Cr-O_{II}, Cr-O_{III} and Cr-Cr distances;

v)   two Debye-Waller factor for the Cr-Cr contribution,$\sigma^2{}_{Cr}$.

The amplitude of the Cr-O_{II} and Cr-O_{III} contributions were defined as:

amp_O_{III} = N(Cr-O_{III}) * $S^0{}_2$ * x

amp_O_{II} = N(Cr-O_{II}) * $S^0{}_2$ * (1-x)

being N(Cr-O_{III}) = 6, N(Cr-O_{II}) = 2, and $S^0{}_2$ = 0.8 (as determined from the analysis of the reference Cr_2O_3). Finally, the Debye-Waller factors for the two Cr-O contributions were fixed to the values found for the two reference phases. This choice was dictated by the strong correlation between σ^2 and coordination numbers N.

The quality of the fits can be appreciated in Figure S8-S11, where the two scattering paths that contribute to the experimental signal are also reported. A summary of the fit results are given in Table 5 of the main text.
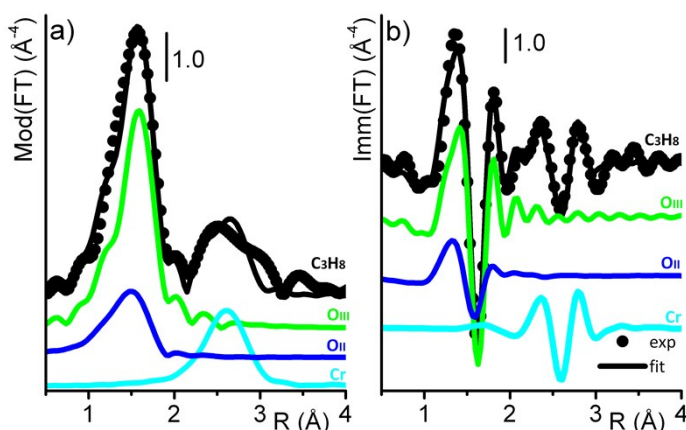

Figure S8 – Phase-uncorrected Fourier Transform (FT) of the $k^3\chi(k)$ EXAFS function for catalyst **1-a**, in both modulus and imaginary parts (parts a and b, respectively); the experimental datum (circles) is overlapped to the best fit (full line) performed with a 2-phases analysis. Also the 3 scattering paths that contribute to the experimental signal are reported (vertically translated for clarity).
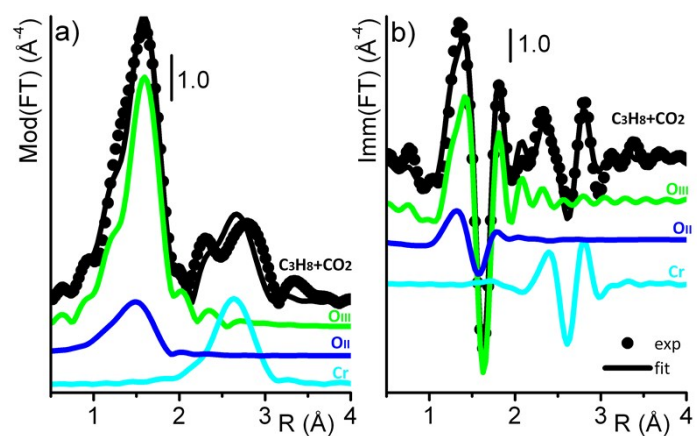
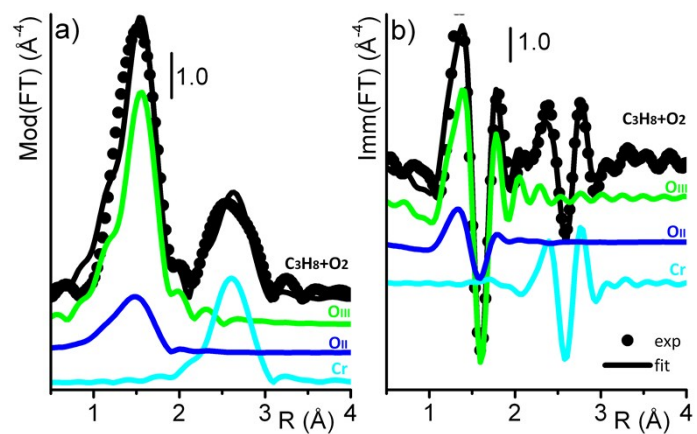Figure S9 –As for Figure S8, for the catalyst **1-b**.

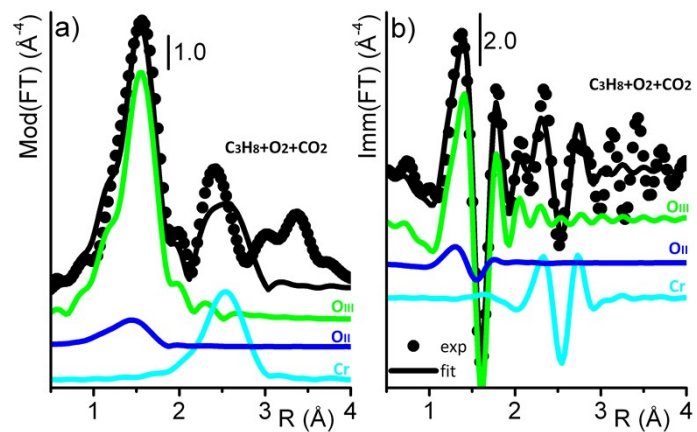Figure S10 –As for Figure S8, for the catalyst **1-c**.

Figure S11 – As for Figure S8, for the catalyst **1-d**.